

MeV-Energy B⁺, P⁺ and As⁺ Ion Implantation into Si

M. Tamura, N. Natsuaki, Y. Wada and E. Mitani

Central Research Laboratory, Hitachi Ltd.

Tokyo 185, Japan

Annealing behavior of secondary defects in 2 MeV B⁺ and P⁺, and 1 MeV As⁺ ion implanted (100) Si is investigated mainly through cross-sectional TEM observations. The defects have peak positions in their depth distributions for both B⁺ (3.2 μm below the surface) and P⁺ (2.1 μm below the surface) implanted layers under all annealing conditions. In contrast, the defects in the layers implanted with As⁺ ions have an almost constant density in their depth distribution and change their depth position with annealing temperature and time. The density and complicated configurations of these defects are significantly reduced by rapid thermal annealing at 1250°C, 90 s. However, the complete elimination of these defects is not realized.

1. Introduction

High energy (≥ 1 MeV) ion implantation into Si substrates using MeV ion beams has made possible the formation of some novel device structures¹⁾. The typical feature of this technology is that a buried layer with a high concentration of dopants can be created in the region several microns beneath the substrate surface. Together with this process, a buried defect layer is also formed near the high concentration region of implanted impurities. In order to apply MeV energy ion implantation technology to device fabrication, the structure, nature and depth distribution of defects in implanted and annealed materials should be carefully investigated.

This paper reports on both furnace and rapid thermal annealing behavior of secondary defects in 2 MeV B⁺ and P⁺, and 1 MeV As⁺ implanted Si. The depth distribution correlation between primary and secondary defects and impurities is also discussed.

2. Furnace Annealing

2.1 Isochronal annealing

A typical example of cross-section TEM (XTEM) micrographs showing secondary defect generation and distributions in 2×10^{13} , 1×10^{14} and 5×10^{14} ions/cm² implanted and 800°C annealed Si is shown in Fig. 1 for B⁺, P⁺ and As⁺ implantation. From the micrographs, it is understood that the critical dose for generating secondary defects is

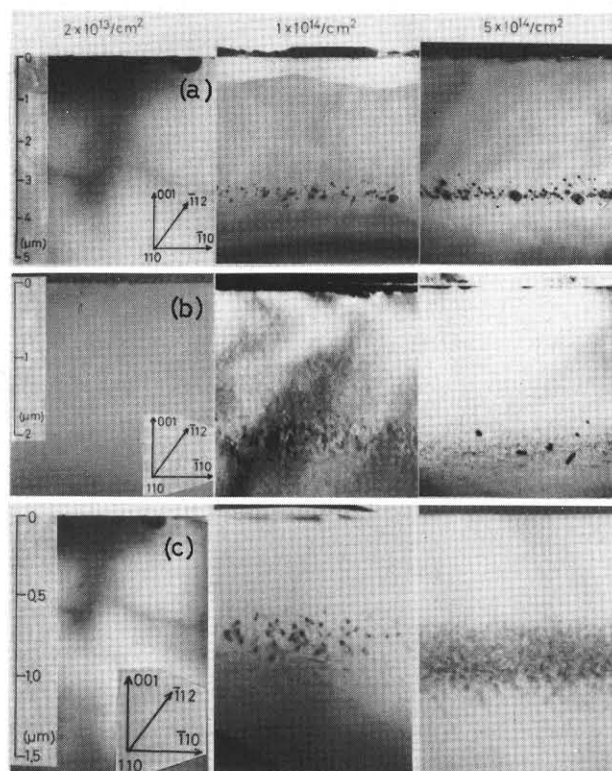


Fig. 1 XTEM micrographs showing secondary defect generation and distributions in 2×10^{13} , 1×10^{14} and 5×10^{14} ions/cm² implanted and 800°C, 15 min annealed Si. (a) 2 MeV B⁺ implantation, (b) 2 MeV P⁺ implantation and (c) 1 MeV As⁺ implantation. Implantation doses are indicated.

between 2×10^{13} and 1×10^{14} ions/cm², independent of ion species. In both B⁺ and P⁺ implanted layers with 1 and 5×10^{14} ions/cm² doses, buried secondary defects such as small dislocation loops and rod-like defects coexist beneath the substrate surface, with maximum densities at depths of around 3.2

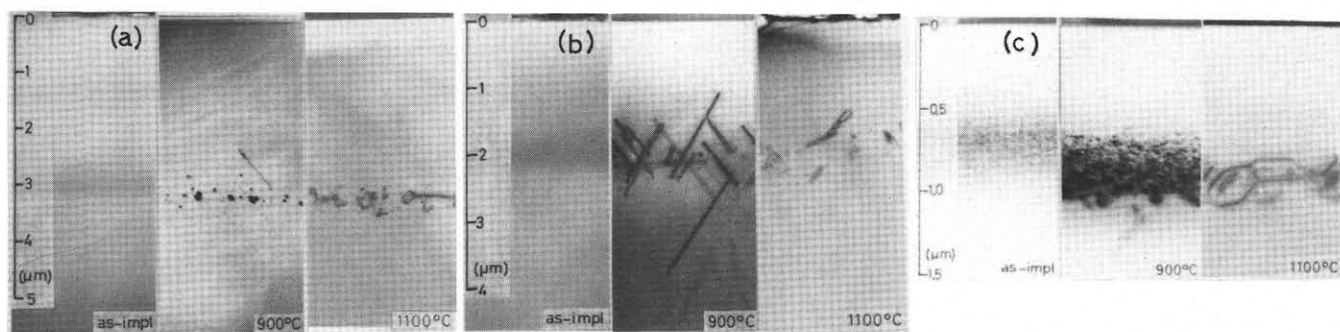


Fig. 2 XTEM micrographs showing 15 min, 900 and 1100°C annealing behavior of secondary defects observed in 5×10^{14} ions/cm² implanted samples together with micrographs of as-implanted samples. Annealing temperatures are indicated. (a) 2 MeV B⁺ implantation (b) 2 MeV P⁺ implantation and (c) 1 MeV As⁺ implantation.

μm (B) and 2.1 μm (P) below the surface. In addition, there are defect-free regions extending from the surface to depths of about 2 μm (B) and 1 μm (P).

In contrast, in the layers implanted with As⁺ ions, two different types of defects are independently distributed. As clearly seen from a micrograph taken for a 5×10^{14} ions/cm² implanted sample, these defects are high density dislocation loops existing between 0.6 and 1.0 μm below the surface and rod-like defects distributed between 1.0 and 1.5 μm below the surface. Moreover, they have an almost constant density in their depth distribution.

In 15 min isochronal annealing of secondary defects observed in 5×10^{14} ions/cm² implanted samples, typical examples of both 900 and 1100°C annealing behavior are shown in Fig. 2, together with results of as-implanted samples. In all the as-implanted layers, no indication of amorphous phase was detected in the diffraction contrast taken from them. However, as seen in the as-implanted micrographs, there are black contrast regions (damage clusters) with peaks near 3 μm (B) and 2 μm (P) depths from the surface. The regions in B⁺ and P⁺ implanted samples show a gradual contrast change into the surface side. On the other hand, damage clusters in an As⁺ implanted layer have a broad distribution from 0.6 to 0.9 μm below the surface. These TEM images of black contrast in as-implanted layers seem to reflect the primary defect distribution in the implanted layer, since nuclear energy deposition density in 2 MeV B⁺ and P⁺, and 1 MeV As⁺ implanted Si shows nearly the same characteristics according to Brice's table²⁾.

Annealing treatment at temperatures above 700

°C produced secondary defects in the implanted layers, although no visible defect formation by TEM was detected at temperatures below 600°C. Both the results of Figs. 1 and 2 clearly show that the positions at which secondary defect density becomes maximum (3.2 μm below the surface for B and 2.1 μm below the surface for P) do not change in these ion implanted layers, even if subsequent higher heat treatment is adopted. These defect positions are slightly deeper than those of damage clusters observed in the as-implanted layers. However, in the As⁺ implanted case, the defects distribute without showing any clear maximum position of defect density.

The vertical widths of such defect distribution vary with annealing temperatures, as can be seen from the micrographs. The defect distribution width became maximum in both B⁺ and P⁺ implanted layers when they were annealed at 900°C, and then became narrow with the increase of annealing temperatures. The vertical defect width in As⁺ implanted layers, however, became gradually narrow as annealing temperatures were increased.

2.2 Isothermal annealing

Under the 1000°C isothermal annealing condition, it was examined whether the depth position of the maximum defect density and the vertical band width of defects can be changed by annealing for a longer time. Figure 3 indicates the vertical band width variation of defects in 5×10^{14} ions/cm² B⁺ and P⁺ implanted layers with annealing time as shown in the figure, although the defect peak position was constant at depths of 3.2 μm (B) and 2.1 μm (P) below the surface.

The shrinkage of the defect band width in both

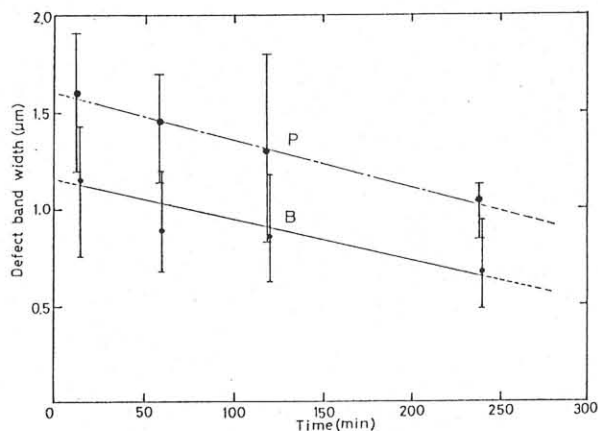


Fig. 3 Vertical band width variation of defects in 2 MeV, 5×10^{14} ions/cm², B⁺ and P⁺ implanted layers with annealing time 15 to 240 min at 1000°C.

B⁺ and P⁺ implanted layers may be due to the following reasons. Since most of the dislocation loops in the band are interstitial in nature³⁾, they shrink by the absorption of vacancies or emission of interstitials. Therefore, one possibility for defect shrinkage is that vacancies flow from the substrate surface to the faults⁴⁾ during annealing in an ambient atmosphere. On the other hand, activation energies of 5.0⁵⁾ and 5.6 eV⁶⁾ have been obtained for the dislocation loop shrinkage in high temperature heat treatment. These values are attributed to an activation energy of the self-diffusion process in Si⁷⁾. That is, the data suggest that Si self-interstitials move to shrink the dislocation loops. Above two mechanisms will work together for defect band shrinkage as a whole with annealing time. However, complete shrinkage, i.e., a total disappearance of defects, was extremely difficult at this temperature. This is probably due to the strong interactions between high density defects in the band. Nearly the same results were obtained for As⁺ implanted layers.

3. Rapid Thermal Annealing

We investigated the effect of high-temperature and short-time annealing on both defect density reduction and defect configuration change by rapid thermal annealing (RTA) treatment. The reason for doing so is that the glide velocity of dislocations and point defect migration from or to dislocations can be fully expected to be dramatically increased at high temperatures of RTA.

Typical XTEM micrographs showing annealing behavior of residual defects by 1250°C heat treatment are indicated in Fig. 4 for annealing times

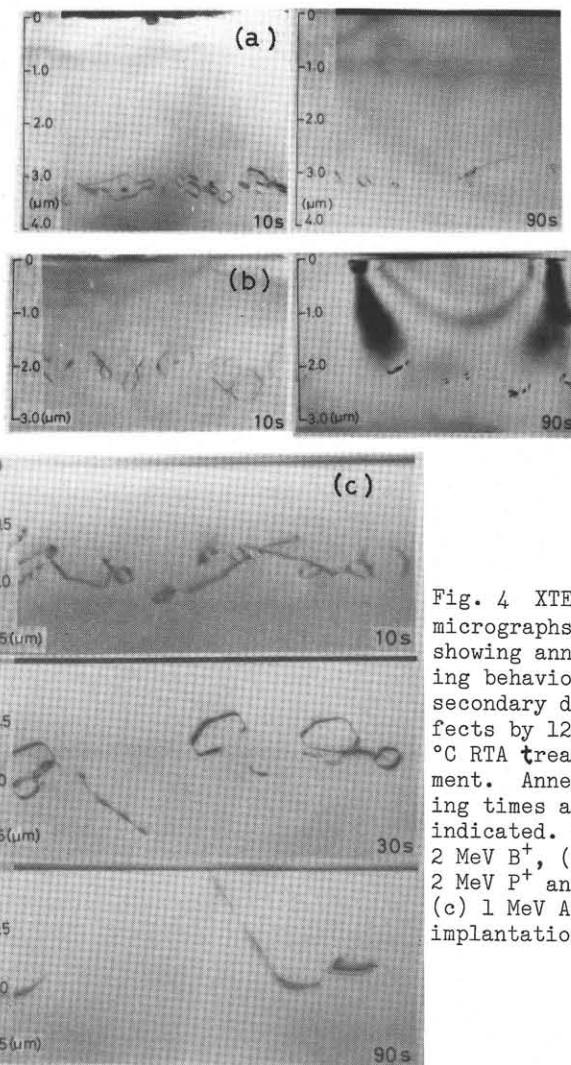


Fig. 4 XTEM micrographs showing annealing behavior of secondary defects by 1250°C RTA treatment. Annealing times are indicated. (a) 2 MeV B⁺, (b) 2 MeV P⁺ and (c) 1 MeV As⁺ implantation.

between 10 and 90 s. Here again we can see that there is a clear difference of defect behavior between B⁺ and P⁺ implantation results and As⁺ implantation ones. The depth positions below the surface where defects in B⁺ and P⁺ implanted layers exist remain unchanged even under such a high temperature annealing condition. In the As⁺ implantation case, however, both the enlargement of dislocation loops and their slight movement toward the surface side can be seen by 1250°C, 30 s annealing. Thus, some dislocation loops reach the substrate surface and slip out from the surface at 1250°C, 90 s.

Instead of dislocation loop movement to the surface, defects in B⁺ and P⁺ implanted samples shrink gradually with annealing time as shown in Fig. 4. This shrinkage rate is much more pronounced than that of 1000°C isochronal annealing, indicating that point defect migration in Si is remarkably enhanced with the increase of annealing temperature from 1000 to 1250°C.

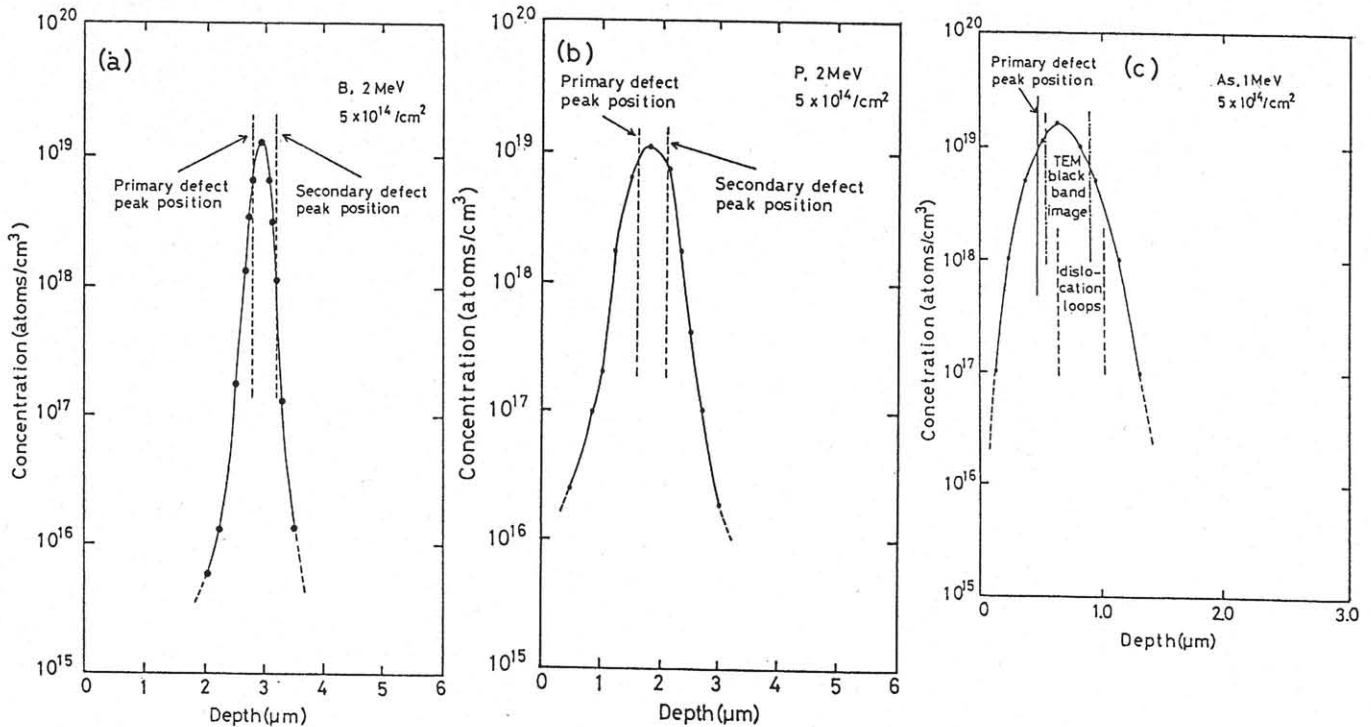


Fig. 5 Impurity concentration profiles of 5×10^{14} ions/cm², B⁺, P⁺ and As⁺ implanted Si followed by 800°C, 15 min annealing by SIMS measurements. Both peaks of nuclear energy deposition density and secondary defects are indicated in 2 MeV B⁺ and P⁺ profiles. Nuclear energy deposition density peak, depth distribution width of damage cluster band in as-implanted layer and depth distribution width of dislocation loops remained after 1000°C, 15 min annealing are indicated in 1 MeV As⁺ profile. (a) 2 MeV B⁺ implantation, (b) 2 MeV P⁺ implantation and (c) 1 MeV As⁺ implantation.

4. Depth Distribution Correlation between Defects and Impurities

Figure 5 shows boron, phosphorus and arsenic concentration profiles of the 5×10^{14} ions/cm² implanted samples followed by 800°C, 15 min annealing by SIMS measurements. On the boron and phosphorus profiles, both peaks of nuclear energy deposition density²⁾ (primary defect density) and secondary defects observed in the present experiment are denoted. Both secondary defect peak positions were constant under all the annealing conditions as stated in the previous sections. As clearly seen from the figures, these defect peak positions in both B⁺ and P⁺ implanted layers exceed projected ranges of B⁺ and P⁺ ions in Si.

On the other hand, one example of distribution width of dislocation loops remaining after 1000°C, 15 min annealing is indicated on the arsenic concentration profile. For reference, a depth distribution width of damage cluster band observed in an as-implanted layer is also denoted on the profile together with a peak of nuclear energy deposition density. The depth of secondary defect distribution also exceeds the position of the projected range, the same as in B⁺ and P⁺ implantation results.

5. Conclusion

Secondary defects in 2 MeV B⁺ and P⁺, and 1 MeV As⁺ ion implanted (100) Si formed after annealing were very stable and difficult to anneal out even after high-temperature (1100°C) and extended (6780 min for both B⁺ and P⁺, and 1200 min for As⁺ at 1000°C) furnace annealing, despite the layers being implanted with a comparatively low dose of 5×10^{14} ions/cm². The density and complicated configurations of these defects were significantly reduced by rapid thermal annealing at 1250°C, 90 s. However, the complete elimination of these defects was not realized.

References

- 1) D. Framanic and M. Current, Sol. State Tech. 27 (1984) 211.
- 2) D. K. Brice, Ion Implantation Range and Energy Deposition Distributions (Plenum, New York, 1975)
- 3) For example, K. Seshan and J. Washburn, Rad. Effects 37 (1978) 147.
- 4) I. R. Sanders and P. S. Dobson, Phil. Mag. 20 (1969) 881.
- 5) T. E. Seidel, D. J. Lischner, C. S. Pai, R. V. Knoell, D. M. Maher and D. C. Jacobson, Nucl. Instr. and Methods B7/8 (1985) 251.
- 6) W. K. Wu and J. Washburn, J. Appl. Phys. 48 (1977) 3747.
- 7) J. M. Fairfield and B. J. Masters, J. Appl. Phys. 38 (1967) 3148.